Silica/Polymer Double-Walled Hybrid Nanotubes: Synthesis and Application as Stimuli-Responsive Nanocontainers in Self-Healing Coatings

Guo Liang Li,[†,*] Zhaoliang Zheng,[†] Helmuth Möhwald,[†] and Dmitry G. Shchukin[†,‡]

[†]Department of Interfaces, Max-Planck Institute of Colloids and Interfaces, 14476 Potsdam, Germany and [‡]Stephenson Institute for Renewable Energy, Department of Chemistry, University of Liverpool, Crown Street, Liverpool L69 7ZD, United Kingdom

ABSTRACT

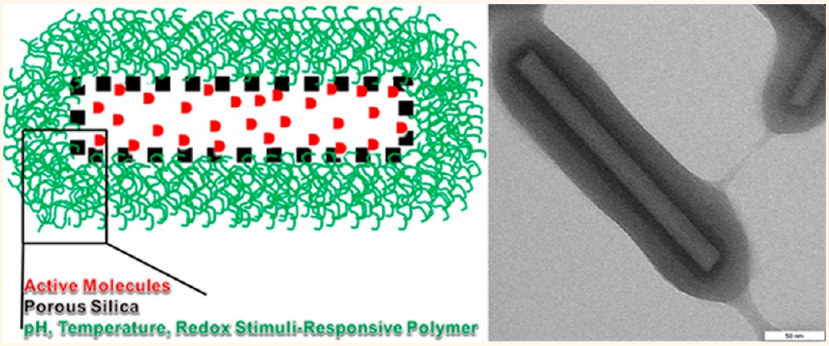

We report the development of silica/polymer double-walled hybrid nanotubes, which consist of a hollow cavity, a porous silica inner wall, and a stimuli-responsive (pH, temperature, and redox) polymeric outer wall, as a novel nanocontainer system. The length, diameter, wall thickness, and aspect ratio of the hybrid nanotubes are precisely controlled in the range of 48—506 nm, 41—68 nm, 3—24 nm, and 1.2—7.6, respectively. The hybrid nanotubes loaded with active molecules exhibit morphology-dependent release and pH-, temperature-, redox-responsive release, which enable a wide range of applications from energy storage to drug delivery and self-healing coatings for metal corrosion protection.

KEYWORDS: hybrid nanotubes · aspect ratio · stimuli-responsive release · self-healing coatings

Metal corrosion protection, one of the most important challenges in the world, is essential to avoid or delay processes causing material destruction. The need for replacement of hazardous chromates in barrier coatings makes "self-healing coatings" of tremendous interest. In addition to a dense barrier, self-healing coatings also provide feedback active healing ability to a scratch on metal surfaces for long-term protection.[1−4] Nanocontainers with controlled release properties can be used in a new family of self-healing coatings. If the environment of the coating changes, smart nanocontainers could quickly respond and release the healing agent onto the metal surfaces to stop corrosion.[5−8] The nanocontainer system always requires defined control of active molecule diffusion in and out of the inner lumen.[9] In other words, it is essential to control encapsulated active molecule release from the cavity to the targeting site as it receives the external environmental signals of pH,[10,11] temperature,[12,13] redox,[14] optical,[15,16] or magnetic field.[17,18]

Hollow tubes which allow active molecules' encapsulation are of great interest in nanotechnology, drug delivery, and energy storage.[19] The carbon nanotubes, found by Lijima in 1991, opened a new era of tube-like material science and have been widely used in many areas.[20] In addition to the carbon materials, silica and organic polymers have always encountered interest because of their easy processing and facile surface modification.[21] Efforts have been

* Address correspondence to guoliang.li@mpikg.mpg.de.

Received for review December 17, 2012 and accepted February 14, 2013.

Published online February 15, 2013
10.1021/nn305814q

devoted to fabricate DNA nanotubes,[22,23] silica nanotubes,[24,25] and polymer-based nanotubes by self-assembly of metal-containing block copolymers.[26−28] The shape of particles is critical to improve their cellular uptake in biological systems.[29−32] In contrast to spherical particles, nonspherical materials could display quite different properties conferred by the morphology. For instance, anisotropic micro/nanocapsules *via* layer-by-layer assembly display improved or enhanced mechanical properties and permeability as containers for controlled release.[33−35] Anisotropic peptide nanotubes with hierarchical structure have even been reported as active optical waveguides.[36,37] Halloysite nanotubes could be tuned in absorption capacity of their lumen for hydrophilic/hydrophobic molecules and purposefully surface modified.[38,39] Nanotube containers are preferable for the continuous, gradual release of active molecules from the cavity for self-healing coatings.[40] However, it is still a challenge to develop tube-like materials with complex inorganic/organic hybrid nanostructures with tunable aspect ratio and flexible surface properties to fit the requirement of various applications, due to the complexity and strict conditions in synthesis procedures.

Herein we report the incorporation of environment-responsive properties into tube-like nanomaterials in self-healing coatings for metal protection. Stimuli-responsive silica/polymer double-walled hybrid nanotubes with controlled aspect ratio (length/diameter) are synthesized by surface-graft precipitation polymerization. The surface grafts on the hybrid nanotubes consist of pH, temperature, or redox-responsive polymers, which confer the hybrid nanotubes' "intelligent" stimuli-responsive properties. In addition to well-defined morphology, uniform size, and wall thickness, the as-prepared silica/polymer hybrid nanotubes exhibit release in response to these different environmental stimuli. The silica/polymer double-walled hybrid nanotubes serve as intelligent nanocontainers to help understand the complex morphology−property relationship, which is very important for the applications in self-healing coatings.

RESULTS AND DISCUSSION

Initially, surface-graft precipitation polymerization was carried out in the presence of double-bond modified nickel-hydrazine/silica core−shell rod templates in acetonitrile resulting in nickel-hydrazine/silica/polymer core-double shell rods. Upon selective etching of the nickel-hydrazine core, well-defined air/silica/polymer hybrid nanotubes with a hollow cavity, a mesoporous silica inner wall and a stimuli-responsive polymer outer wall were obtained. The functional monomers and the cross-linking agents for the surface-graft precipitation polymerization in the present work are shown in Figure 1. The polymerized cross-linked network on hybrid nanotube surfaces is

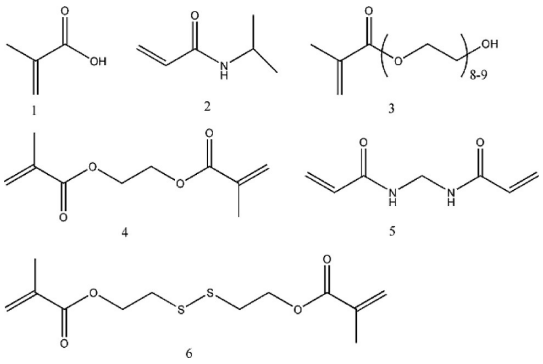

Figure 1. Chemical structure of the monomers (1−3) and the cross-linkers (4−6) for the stimuli-responsive silica/polymer hybrid nanotubes. 1-methacrylic acid, 2-*N*-isopropylacrylamide, 3-poly(ethylene glycol) methacrylate, 4-ethylene glycol dimethacrylate, 5-*N*,*N*′-methylenebisacrylamide and 6-bis(2-methacryloyl)oxyethyl disulfide.

poly(methacrylic acid-*co*-ethylene glycol dimethacrylate), poly(*N*-isopropylacrylamide-*co*-methylenebisacrylamide) and poly(poly(ethylene glycol) methacrylate-*co*-bis(2-methacryloyl)oxyethyl disulfide), which enables the response to environmental pH, temperature and changes of redox potential, respectively.

The silica nanotubes without polymer outer wall were obtained by removal of nickel-hydrazine rod templates (Table S1, Supporting Information). These silica nanotubes have almost the same diameter of ca. 38 nm and wall thickness of ca. 9 nm. Only the length of silica nanotubes changes from 41 nm to 125, 215, 237, and 480 nm. Thus, the aspect ratio (aspect ratio = length/diameter) varies between1.2 and 10.2. Figures 2A and 2B show typical TEM images of the as-prepared silica nanotubes with aspect ratio of 1.2 and 6.0, respectively. The surface-graft precipitation polymerization was performed to obtain silica/polymer hybrid nanotubes with a stimuli-responsive polymer outer wall. The silica/PMAA hybrid nanotubes with controllable L/D aspect ratio and wall thickness obtained from different aspect ratio nickel-hydrazine/silica templates in surface-graft precipitation polymerization are summarized in Table 1. First well-defined and pH-responsive silica/PMAA hybrid nanotubes were synthesized and characterized. The hybrid nanotubes exhibit a length ranging from 48 to 506 nm and diameter from 41 to 68 nm, which have a tunable aspect ratio between 1.2 and 7.6. Typical TEM images of the silica/PMAA nanotubes with a L/D ratio 4.0 are shown in Figures 2C and 2D. They exhibit clear double walled hollow nanostructures, comparable to that of ungraft silica nanotubes (Figures 2A and 2B). Moreover, the wall thickness of grafted polymers can be well controlled as the feed ratio of monomer to the silica templates is adjusted.[41] For instance, the thickness of the PMAA outer wall increases from 9 to 15 nm (Figure 2E) when the feed ratio increases from 3 to 4.

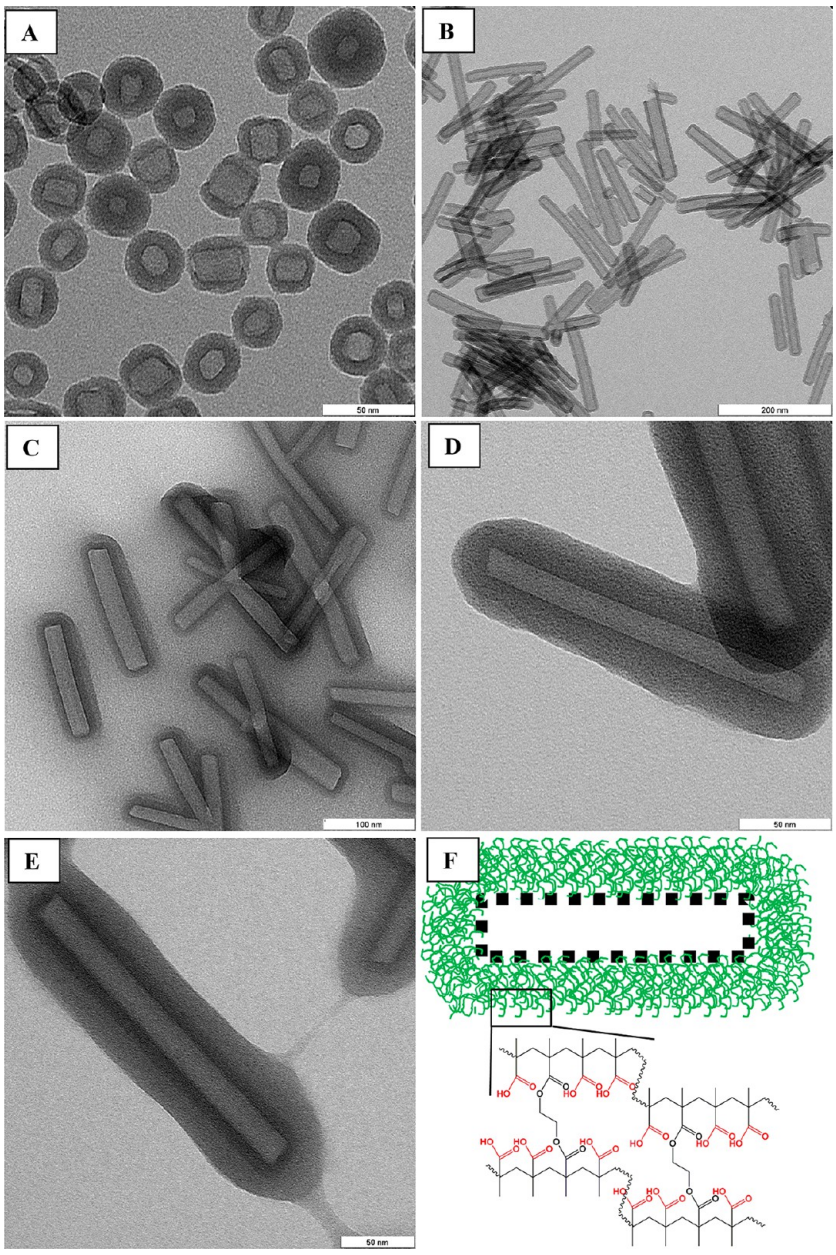

Figure 2. TEM images and schematic structure of the silica hollow nanotubes (A and B) and silica/polymer hybrid hollow nanotubes (C–F) with surface grafting of pH-responsive poly(methacrylic acid) (PMAA) polymer networks (A and B are the silica nanotubes, C and D are the SiO_2/PMAA-2 nanotubes, and E is the SiO_2/PMAA-3 nanotube in Table 1). The nickel-hydrazine rod templates were selectively removed by HCl treatment. The scale bars in Figure A-E are 50, 200, 100, 50, 50 nm, respectively.

BET was carried out to check the porous structure of the silica inner walls of the silica/PMAA hybrid nanotubes (Figure S1 and Table S2, Supporting Information). The porous silica wall has a mean pore size of 3.7 nm and a pore volume of 1 - 1.6 cm^3/g. Compared to that of the ungrafted silica nanotubes, the FT-IR absorption spectrum of the silica/PMAA hybrid nanotubes presents the stretching vibration of carboxyl groups (peaks at 1720 and 1160 cm^{-1} attributable to the stretching vibration of C═O and C–O groups from the PMAA segments, respectively, Figure S2, Supporting Information). The zeta-potential (ζ) of the silica/PMAA hybrid nanotubes with −41.1 mV suggests that the surface-grafted PMAA on the nanotubes endows the resultant silica/PMAA hybrid nanotubes high stability in deionized (DI) water as compared to that of surface ungrafted silica nanotubes of −0.6 mV in aqueous solution. Thus, as-prepared silica/PMAA hybrid nanotubes consist of an interior cavity for active molecule encapsulation, a mesoporous silica inner wall and a pH-responsive PMAA outer wall for the transport control of active molecules in and out of the containers.

We further apply the above well-defined silica/PMAA hybrid as a novel smart container system. Since

TABLE 1. Stimuli-Responsive Silica/Polymer Hybrid Nanotubes with Tunable Aspect Ratio

entry	L/D^b	length (L, nm)^c	diameter (D, nm)^c	wall thickness (h, nm)^d
SiO_2/PMAA1[a]	1.2	48	41	9/3
SiO_2/PMAA2	4.0	225	56	9/9
SiO_2/PMAA3	4.2	292	68	9/15
SiO_2/PMAA4	7.6	506	67	11/10
SiO_2/PNIPAM[a]	5.7	246	43	9/5
SiO_2/PPEGMA[a]	6.0	245	41	9/3

[a] Surface-graft precipitation polymerization was performed in acetonitrile to obtain a controllable cross-linked polymer outer wall by varying the (monomer+cross-linker)/silica feed ratio 2—4 by weight. The initiator AIBN was 1.5 wt % relative to the total amount of monomer and cross-linker. For the silica/PMAA, silica/PNIPAM and silica/PPEGMA nanotubes, the cross-linker is ethylene glycol dimethacrylate, *N,N′*-methylenebisacrylamide, and bis(2-methacryloyl)oxyethyl disulfide, respectively. [b] The aspect ratio was calculated by the length/diameter (L/D) of the nanotubes. [c] The length and diameter of the nanotubes were measured from the TEM images, the coefficient of variation (the ratio of standard deviation to the mean) is 3—10%. [d] The wall thickness includes both of the silica inner wall/polymer outer wall.

the benzotriazole (BTA) molecule is a well-known anticorrosion inhibitor that anchors onto the metal surface to prevent corrosion occurrence, BTA molecules were selected as a model probe to be encapsulated in the present work. The loading and release dynamics of the BTA in the cavity of the silica/PMAA hybrid nanotubes were studied at different pH values. The silica/PMAA hybrid nanotubes were dispersed in a BTA/acetone solution (80 mg/mL) to form a homogeneous suspension. The loading of the BTA molecules into the SiO_2/PMAA hybrid nanotubes was then performed in vacuum to enhance the loading efficiency. The loading capacity of the hybrid nanotubes was found 6—7% by weight.

For a comparative study the release dynamics of the SiO_2/PMAA hybrid nanocontainers with an aspect ratio of 4.0 and 7.6 (SiO_2/PMAA 2 and SiO_2/PMAA 4, respectively, in Table 1) were monitored by fluorescence spectroscopy. Figure 3A shows the release profiles of BTA from the hybrid nanotubes in pH 7 aqueous solution. It indicates that the active molecules of BTA were released faster from the SiO_2/PMAA 4 hybrid nanotubes than from SiO_2/PMAA 2 hybrid nanotubes at the same environmental solutions. It is comparable with our previous study of halloysite-based containers.[40] The active molecules could only be released from the edges of the halloysite clay nanotubes, which results in a geometry-restricted release rate. For the present work, the fast release from the silica/PMAA 4 hybrid nanotubes is probably dominated by defects in the nanotube walls (Figure S3, Supporting Information). These defects could be formed during the silica rod fabrication and the etching process for template removal. The nanotubes with higher aspect ratios are more prone to breaking than shorter ones. The defects in the hybrid nanotubes

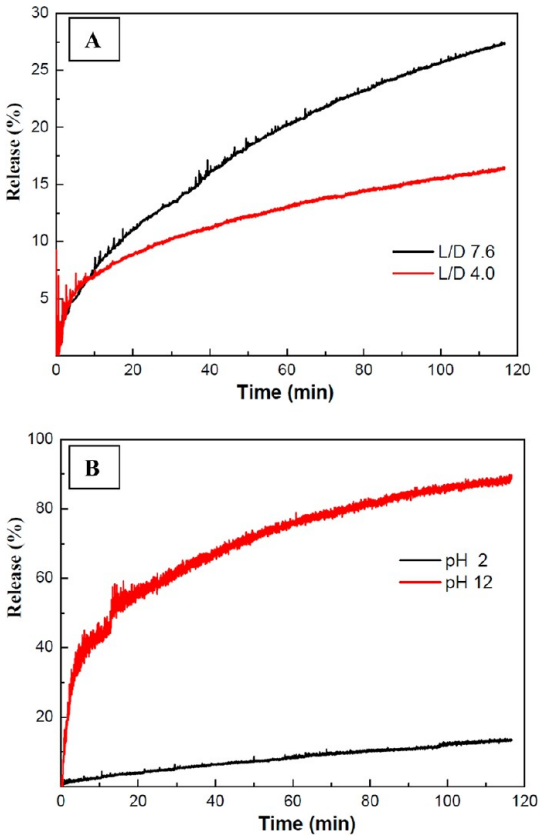

Figure 3. Release dynamics of benzotriazole from the silica/PMAA hybrid nanotubes with different L/D aspect ratio at pH 7 (A) and at HCl (pH 2) and NaOH (pH 12) solutions (B).

with higher aspect ratio result in fast release of the active BTA molecules.

The BTA-loaded hybrid nanotubes were also tested in aqueous solutions at different pH in order to investigate the stimuli-responsiveness. Figure 3B shows that the BTA molecules at pH 12 are released faster from the SiO_2/PMAA 4 hybrid nanotube hollow cavity than at pH 2. During the release of the active molecules out of the nanotubes, the pH-responsive PMAA outer walls play an important role. At low pH, the PMAA outer wall is protonated and the uncharged carboxylic acid groups allow aggregation of the polymer chains to block the active BTA diffusion out of the polymer outer wall. At pH 12, the carboxylic acid groups on the hybrid nanotubes are deprotonated. The anionic polymer chains change from the shrunk state to a highly swollen state and thus release the BTA molecules. Moreover, the TEM image of the SiO_2/PMAA hybrid nanotubes in Figure 4 treated at pH 12 suggests that the silica inner wall is dissociated under the condition of highly alkaline solution.[42] The corrosion process is accompanied by pH changes, which could trigger the release of the anticorrosion inhibitor to heal the metal surfaces. Thus, the pH-dependence of the release from hybrid nanotube containers could lead to self-healing coatings for metal corrosion protection.

In addition to the pH-responsive PMAA outer wall on the hybrid nanotubes, the temperature-responsive PNIPAM and redox-responsive PPEGMA polymers have been polymerized on the hybrid nanotubes by surface-graft precipitation polymerization. The TEM images of the as-obtained SiO_2/PNIPAM and SiO_2/PPEGMA hybrid nanotubes are shown in Figures 5A and 5C, respectively. The PNIPAM polymer is a well-known thermosensitive material, which could be applied to a temperature triggered release from the nanocontainers.[43] The dynamic release of BTA-loaded SiO_2/PNIPAM containers in Figure 6A shows a temperature-dependent activity. At a low temperature of 25 °C, the PNIPAM outer wall is swollen. At high temperature of 50 °C (>LCST), the PNIPAM outer wall tends to shrink, which blocks the BTA molecules in the cavity to diffuse out of the shell. For the SiO_2/PPEGMA hybrid nanocontainer, the PEG chains and disulfide bonds in the silica/PPEGMA hybrid nanotubes endow the containers biocompatibility and redox-sensitivity, respectively. The release profile of the BTA-SiO_2/PPEGMA hybrid nanocontainers in the presence of redox-active 1 mM DL-dithiothreitol (DTT) is shown in Figure 6B. In comparison to the release rate without the reductive agent DTT, the BTA-SiO_2/PPEGMA nanocontainers in 1 mM DTT is high. This could be explained by breaking of the disulfide bonds in the PPEGMA outer wall in the presence of DTT reducing agent.[44] Thus, the cross-linked PPEGMA outer wall changes into linear PPEGMA chains (un-cross-linked outer wall) in DTT solution, which results in a fast release of BTA from the cavity of the SiO_2/PPEGMA hybrid nanotubes. The incorporation of

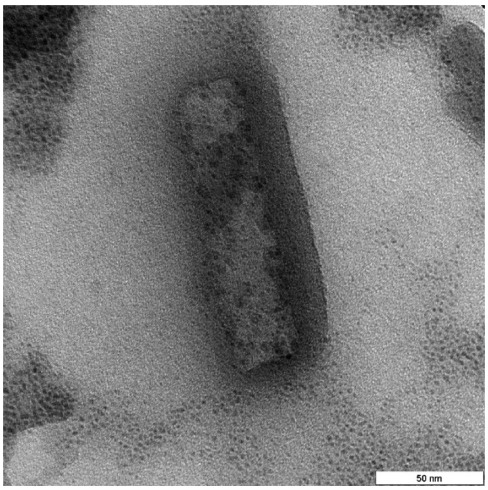

Figure 4. TEM image of the silica/PMAA nanocontainer under the condition of pH 12 aqueous solution over a period of 2 h. The silica inner wall was dissociating slowly as it was exposed to the sodium hydroxide, which resulted in a fast release of encapsulated BTA in the cavity of the hybrid nanotubes.

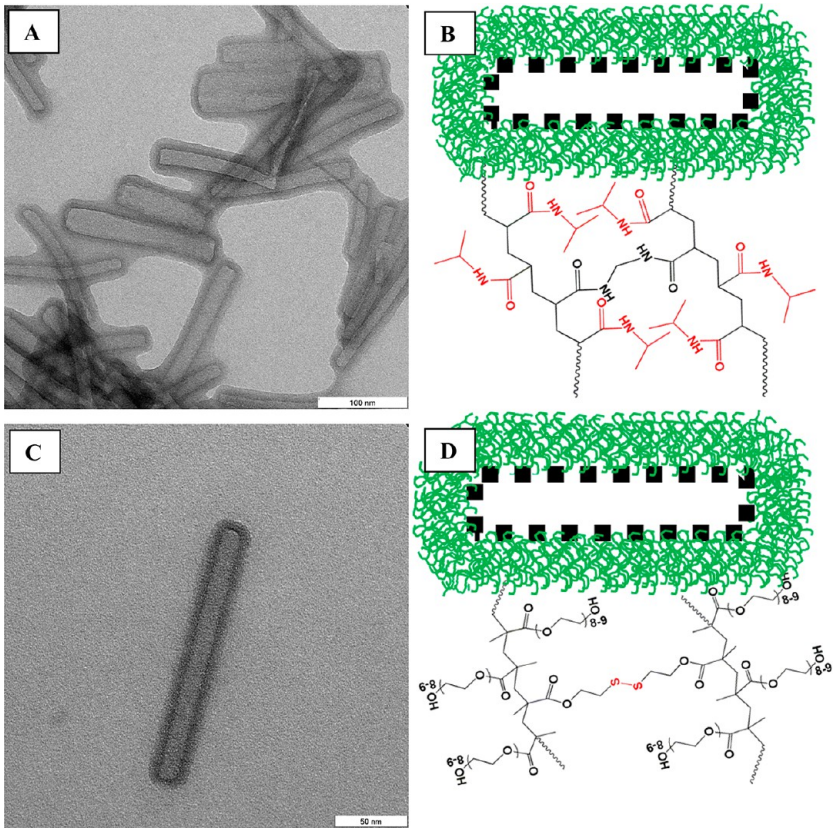

Figure 5. TEM images and scheme of the temperature-responsive silica/PNIPAM (A and B) and redox-responsive silica/PPEGMA (C and D) hybrid nanotubes. The scale bar in A and C is 100 and 50 nm, respectively.

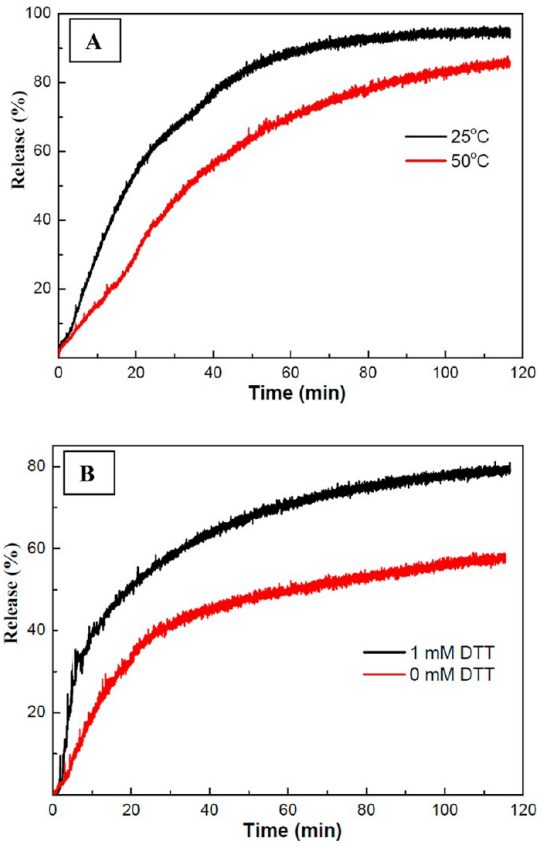

Figure 6. Release dynamics of benzotriazole from the silica/PNIPAM (A) and the silica/PPEGMA (B) hybrid nanotubes.

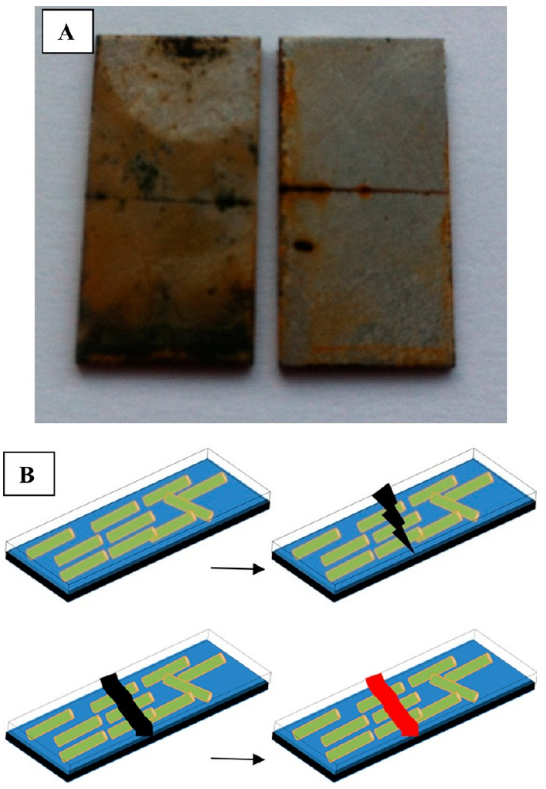

Figure 7. (A) Corrosion test: carbon steel coated with a pure SiO_x/ZrO_y film (left) and a SiO_x/ZrO_y film doped with BTA-loaded silica/PMAA nanotube containers (right) after immersion in 0.1 M NaCl for 48 h; (B) the self-healing mechanism of anticorrosion coatings on metal surfaces. When coatings on the metal surface are attacked, the coatings will be broken and could not serve as dense barrier to block corrosion species. But the coatings with inhibitor-loaded nanotube containers could terminate corrosion, since the increase of pH around corrosion sites motivates fast releases of the inhibitor from the nanocontainers to from a thin film on the metal surfaces. (The black line means that the metal surface is exposed to the air under attack; the red line means that corrosion-inhibitors form a thin film on metal surfaces).

cleavable disulfide bonds into the container system is of great importance to affect living cells, gene silencing and therapy.[45]

The BTA-loaded SiO_2/PMAA nanotube containers were doped into a SiO_x/ZrO_y film to obtain self-healing coatings on carbon steel. Figure 7A shows a preliminary corrosion test of carbon steel with a pure sol–gel coating and self-healing coating, respectively. In contrast to the pure sol–gel coating (Figure 7A left), the self-healing coating with BTA-loaded SiO_2/PMAA nanotube containers (Figure 7A right) displayed an enhanced corrosion protection. The mechanism of the self-healing anticorrosion is shown in Figure 7B. As the coating on the metal surface is attacked or scratched, the coatings could not serve a dense barrier to block corrosion species any more. But the self-healing coating with corrosion inhibitor-loaded nanotube containers could delay the corrosion process effectively. In addition to the fast release of BTA from the broken tube nanocontainers, the BTA molecules from the unbroken containers around the scratched areas can also be released quickly to prevent further corrosion occurrence due to the pH changes.[6] This facilitates a self-motivated release of the healing agent from the nanocontainers in self-healing coatings. Thus, the fast release of corrosion inhibitor (BTA) from nanocontainers to the scratched metal surfaces in self-healing coatings prevented pH changes in the metal surface coating and avoided further corrosion.

CONCLUSIONS

A general approach to stimuli-responsive silica/PMAA, silica/PNIPAM, and silica/PPEGMA hybrid nanotubes with tunable diameter, length, aspect ratio, wall thickness, and surface chemistry by surface-graft precipitation polymerization has been demonstrated. In addition to the unique nanostructures, the as-obtained silica/polymer hybrid nanotubes have been shown to be promising as a nanocontainer system for self-healing coatings in corrosion control. The anticorrosion agent benzotriazole encapsulated in the hybrid nanotubes can be controlled to be released in the absence and presence of external stimuli: (i) the silica/PMAA hybrid nanotubes reveal pH-dependent release of the benzotriazole because of the carboxylic acid groups from the PMAA outer wall; (ii) the silica/PNIPAM hybrid

nanotubes exhibit a temperature-dependent release because of the grafted PNIPAM polymers; (iii) the silica/PPEGMA hybrid nanotubes show a redox-dependent release because of the existence of disulfide bonds in the PPEGMA polymer networks. The developed pH-, temperature-, and redox-responsive silica/polymer hybrid nanotubes present a new, functional, and "intelligent" nanocontainer system for corrosion protection coatings. The proposed universal approach for the synthesis of surface-active and tube-like hybrid nanomaterials will serve to construct promising building blocks for various future applications.

METHODS

Materials. Tetraethyl orthosilicate (TEOS), 3-(trimethoxysilyl) propyl methacrylate (98%), *N*-isopropylacrylamide (NIPAM), ethylene glycol dimethacrylate (EGDMA, 98%), poly(ethylene glycol) methacrylate (PEGMA, M_w 360), bis(2-methacryloyl)oxyethyl disulfide, and D,L-dithiothreitol (DTT) were purchased from Sigma-Aldrich. Brij 58, cyclohexane (99.5%), and methacrylic acid (MAA, 99.5%) were purchased from Acros. Azobis(isobutyronitrile) (AIBN) and *N*,*N*′-methylenebisacrylamide (MBA) were purchased from Fluka. Monomers of MAA, PEGMA, and EGDMA were passed through an inhibitor-removal column to remove inhibitor and stored in argon at −10 °C. The inhibitor removers were packed in a column for removing hydroquinone monomethyl ether (Sigma-Aldrich, dimensions: 9 × 0.8 in.). AIBN and NIPAM were recrystallized in methanol and hexane, respectively.

Synthesis of Silica/Polymer Hybrid Nanotubes. First, the nickel hydrazine/silica core−shell rod templates were synthesized.[46] The as-synthesized rod templates were further surface-modified with 3-(trimethoxysilyl)propyl methacrylate to introduce carbon−carbon double bonds on the silica surfaces. These double bonds serve as grafting sites for the following polymer coating. Briefly, 0.5 g of the nickel hydrazine/silica core−shell rods was dispersed in 20 mL of isopropyl alcohol, and 1 mL of 3-(trimethoxysilyl)propyl methacrylate was introduced into the above solution. The surface modification process was allowed to proceed for 48 h at room temperature, and the rods were collected by two dispersion/centrifugation cycles (at 12 000 rpm for 30 min, in an SIGMA 3-30k centrifuge). Surface-modified nickel hydrazine/silica core−shell rod templates with a length to diameter (*L*/*D*) ratio of 1.2, 3.5, 5.6, 6, and 10.2 were thus obtained.

The coating of stimuli-responsive polymers on nickel hydrazine/silica core−shell rods was carried out by surface-grafted precipitation polymerization in acetonitrile. In a typical synthesis, the surface-modified nickel hydrazine/silica core−shell rod template was dispersed in acetonitrile (4 mg/mL) by sonication for 15 min. The monomer MAA (0.5 mL, 6 mmol), cross-linker EGDMA (0.12 mL, 0.6 mmol), and initiator AIBN (1.5 wt % relative to the total amount of monomer and cross-linker) were then added to the modified silica template solution. The surface-graft precipitation polymerization was carried out in reflux conditions for 4 h. The as-obtained nickel hydrazine/silica/PMAA core−double shell rods were washed with acetonitrile and tetrahydrofuran. The PMAA grafting thickness was simply controlled by varying the feed ratio between monomer and nickel hydrazine/silica templates. The thickness of the PMAA outer wall increased from 3 to 9 to 15 nm when the feed ratio increased from 2 to 3 and 4 (Table 1).

Finally, silica/polymer hybrid nanotubes were prepared *via* selective etching of the nickel hydrazine/silica/polymer core−double shell rods in HCl solution (1 M), followed by repeated washes with DI water to a constant pH.

Corrosion Inhibitor-Loaded Hybrid Nanotubes and Release Dynamics. To encapsulate corrosion inhibitor of benzotriazole (BTA) in SiO_2/PMAA hybrid nanotubes, the hybrid nanotubes were mixed with a saturated solution of BTA in acetone (80 mg/mL). Then, the suspension was kept under vacuum for 3 h, centrifuged, and washed with DI water. The above loading process was repeated three times in order to increase the loading efficiency. The loaded BTA content in nanotubes was determined by UV−vis spectroscopy using analytical curves obtained at pure BTA standard concentration ranging from 10^{-3}−10^{-1} mg/mL in DI water. The BTA-loaded hybrid nanotubes were dispersed in DI water and monitored at an absorption wavelength of 275 nm for the UV−vis measurement in the following 2 weeks. The loading capacity was calculated according to the equation below.

$$\text{loading capacity}\ (\%) = \text{mass of BTA molecules in nanotubes} / (\text{mass of BTA molecules in nanotubes} + \text{mass of nanotubes})$$

The release dynamics was investigated in DI water at different pH solutions. The BTA-loaded hybrid nanotube suspension was constantly stirred with a magnetic stir bar during the release process. The initial concentration of the BTA-loaded SiO_2/PMAA hybrid nanotubes was 1 mg/mL, and then the release of BTA from the cavity of the nanotubes was monitored *via* the fluorescence spectra. The release dynamics of BTA from hybrid nanotubes in water were monitored *via* the fluorescence intensity following excitation at a wavelength of 358 nm.

Self-Healing Coatings for Corrosion Protection. The self-healing coatings were prepared by dispersing the as-obtained nanotube containers into SiO_x/ZrO_y hybrid films at room temperature. Prior to coating, the carbon steel substrates (1 × 2 cm) were polished, degreased with acetone, and washed with DI water. The SiO_x/ZrO_y hybrid films doped with benzotriazole-loaded SiO_2/PMAA nanocontainers were prepared by a sol−gel process. Briefly, the zirconium oxide sol was prepared by hydrolyzing zirconium *n*-propoxy solution (TPOZ, 70 wt % 2-propanol) in ethylacetoacetate (1:1 v/v) at room temperature for 20 min. The second organosiloxane sol was prepared by hydrolyzing CPTMS in 2-propanol by the addition of acidified water (HNO_3, pH 0.5) for 20 min. Then, the zirconia sol and organosiloxane sol were mixed (1:2 v/v) and stirred for 60 min and aged for 1 h at room temperature. The BTA-loaded nanotube containers were mixed with the SiO_x/ZrO_y films with a concentration of 10 mg/mL by sonication. The self-healing films on carbon steel were fabricated by a dip-coating procedure. The carbon steel was immersed into the sol−gel mixtures for 120 s and then was withdrawn at a speed of 18 cm/min. Finally, the samples were cured at 130 °C for 1 h.

Characterization. The morphology and size of the hybrid nanotubes were characterized by transmission electron microscopy (TEM, Zeiss EM912 Omega). Samples were dispersed in solvent, and a drop of the dispersion was spread onto the surface of a copper grid coated with a carbon membrane and then dried in vacuum at room temperature for TEM characterization. The Brunauer−Emmett−Teller (BET) adsorption/desorption isotherm was determined by nitrogen sorption at 77 K using a Micromeritics ASAP 2000 surface area analyzer. The pore size and size distribution were obtained by the DFT method. Fourier transform infrared (FT-IR) spectroscopy was carried out with a Varian 1000 FT-IR (Scimitar Series) spectrophotometer. Zeta-potential was measured in aqueous solution (0.5 mg/mL) by ZetaSizer Nano ZS (Malvern Instruments). The BTA inhibitor loading efficiency and release kinetics were determined *via* absorption (8453 UV−visible spectrophotometer, Agilent Technologies) and fluorescence (FluoroMax-4, HORIBA Jobin Yvon) techniques.

Conflict of Interest: The authors declare no competing financial interest.

Acknowledgment. G. L. Li acknowledges support by a research fellowship from Alexander von Humboldt Foundation and support from the EUFP7 "nanocarrier" project. We thank Dimitriya Borisova for the SEM images, Rona Pitschke for the TEM images, Dr. Xiaofeng Liu for the FT-IR spectra, and

Dr. Dilek Akcakayiran for the BET measurement. We also thank Dr. Xuehai Yan for helpful discussions.

Supporting Information Available: TEM images, FT-IR and BET results of the silica/polymer double-walled hybrid nanotubes. This material is available free of charge *via* the Internet at http://pubs.acs.org.

REFERENCES AND NOTES

1. White, S. R.; Sottos, N. R.; Geubelle, P. H.; Moore, J. S.; Kessler, M. R.; Sriram, S. R.; Brown, E. N.; Viswanathan, S. Autonomic Healing of Polymer Composites. *Nature* **2001**, *409*, 794–797.
2. Toohey, K. S.; Sottos, N. R.; Lewis, J. A.; Moore, J. S.; White, S. R. Self-Healing Materials with Microvascular Networks. *Nat. Mater.* **2007**, *6*, 581–585.
3. Cho, S. H.; White, S. R.; Braun, P. V. Self-Healing Polymer Coatings. *Adv. Mater.* **2009**, *21*, 645–649.
4. Odom, S. A.; Chayanupatkul, S.; Blaiszik, B. J.; Zhao, O.; Jackson, A. C.; Braun, P. V.; Sottos, N. R.; White, S. R.; Moore, J. S. A Self-Healing Conductive Ink. *Adv. Mater.* **2012**, *24*, 2578–2581.
5. Shchukin, D. G.; Mohwald, H. Smart Nanocontainers as Depot Media for Feedback Active Coatings. *Chem. Commun.* **2011**, *47*, 8730–8739.
6. Shchukin, D. G.; Zheludkevich, M.; Yasakau, K.; Lamaka, S.; Ferreira, M. G. S.; Mohwald, H. Layer-by-Layer Assembled Nanocontainers for Self-Healing Corrosion Protection. *Adv. Mater.* **2006**, *18*, 1672–1678.
7. Borisova, D.; Mohwald, H.; Shchukin, D. G. Mesoporous Silica Nanoparticles for Active Corrosion Protection. *ACS Nano* **2011**, *5*, 1939–1946.
8. Kendig, M.; Hon, M.; Warren, L. `Smart' Corrosion Inhibiting Coatings. *Prog. Org. Coat.* **2003**, *47*, 183–189.
9. Stuart, M. A. C.; Huck, W. T. S.; Genzer, J.; Muller, M.; Ober, C.; Stamm, M.; Sukhorukov, G. B.; Szleifer, I.; Tsukruk, V. V.; Urban, M.; *et al.* Emerging Applications of Stimuli-Responsive Polymer Materials. *Nat. Mater.* **2010**, *9*, 101–113.
10. Kim, K. T.; Meeuwissen, S. A.; Nolte, R. J. M.; van Hest, J. C. M. Smart Nanocontainers and Nanoreactors. *Nanoscale* **2010**, *2*, 844–858.
11. Kim, K. T.; Cornelissen, J. J. L. M.; Nolte, R. J. M.; van Hest, J. C. M. A Polymersome Nanoreactor with Controll able Permeability Induced by Stimuli-Responsive Block Copolymers. *Adv. Mater.* **2009**, *21*, 2787–2791.
12. Yoshimatsu, K.; Lesel, B. K.; Yonamine, Y.; Beierle, J. M.; Hoshino, Y.; Shea, K. J. Temperature-Responsive "Catch and Release" of Proteins by using Multifunctional Polymer-Based Nanoparticles. *Angew. Chem., Int. Ed.* **2012**, *51*, 2405–2408.
13. Rahman, M. M.; Elaissari, A. A Versatile Method for the Preparation of Rigid Submicron Hollow Capsules Containing a Temperature Responsive Shell. *J. Mater. Chem.* **2012**, *22*, 1173–1179.
14. Cho, H.; Bae, J.; Garripelli, V. K.; Anderson, J. M.; Jun, H. W.; Jo, S. Redox-Sensitive Polymeric Nanoparticles for Drug Delivery. *Chem. Commun.* **2012**, *48*, 6043–6045.
15. Klinger, D.; Landfester, K. Photo-sensitive PMMA Microgels: Light-Triggered Swelling and Degradation. *Soft Matter* **2011**, *7*, 1426–1440.
16. Chung, J. W.; Lee, K.; Neikirk, C.; Nelson, C. M.; Priestley, R. D. Photoresponsive Coumarin-Stabilized Polymeric Nanoparticles as a Detectable Drug Carrier. *Small* **2012**, *8*, 1693–1700.
17. Kulbaba, K.; Cheng, A.; Bartole, A.; Greenberg, S.; Resendes, R.; Coombs, N.; Safa-Sefat, A.; Greedan, J. E.; Stover, H. D. H.; Ozin, G. A.; *et al.* Polyferrocenylsilane Microspheres: Synthesis, Mechanism of Formation, Size and Charge Tunability, Electrostatic Self-Assembly, and Pyrolysis to Spherical Magnetic Ceramic Particles. *J. Am. Chem. Soc.* **2002**, *124*, 12522–12534.
18. Bhattacharya, S.; Eckert, F.; Boyko, V.; Pich, A. Temperature-, pH-, and Magnetic-Field-Sensitive Hybrid Microgels. *Small* **2007**, *3*, 650–657.
19. Ai, S. F.; Lu, G.; He, Q.; Li, J. B. Highly Flexible Polyelectrolyte Nanotubes. *J. Am. Chem. Soc.* **2003**, *125*, 11140–11141.
20. Iijima, S. Helical Microtubules of Graphitic Carbon. *Nature* **1991**, *354*, 56–58.
21. Hoffmann, F.; Cornelius, M.; Morell, J.; Froba, M. Silica-Based Mesoporous Organic–Inorganic Hybrid Materials. *Angew. Chem., Int. Ed.* **2006**, *45*, 3216–3251.
22. Wilner, O. I.; Orbach, R.; Henning, A.; Teller, C.; Yehezkeli, O.; Mertig, M.; Harries, D.; Willner, I. Self-Assembly of DNA Nanotubes with Controllable Diameters. *Nat. Commun.* **2011**, *2*, 540.
23. Wilner, O. I.; Henning, A.; Shlyahovsky, B.; Willner, I. Covalently Linked DNA Nanotubes. *Nano Lett.* **2010**, *10*, 1458–1465.
24. Mullner, M.; Yuan, J. Y.; Weiss, S.; Walther, A.; Fortsch, M.; Drechsler, M.; Muller, A. H. E. Water-Soluble Organo-Silica Hybrid Nanotubes Templated by Cylindrical Polymer Brushes. *J. Am. Chem. Soc.* **2010**, *132*, 16587–16592.
25. Mullner, M.; Lunkenbein, T.; Breu, J.; Caruso, F.; Muller, A. H. E. Template-Directed Synthesis of Silica Nanowires and Nanotubes from Cylindrical Core–Shell Polymer Brushes. *Chem. Mater.* **2012**, *24*, 1802–1810.
26. Wang, X. S.; Wang, H.; Coombs, N.; Winnik, M. A.; Manners, I. Redox-Induced Synthesis and Encapsulation of Metal Nanoparticles in Shell-Crosslinked Organometallic Nanotubes. *J. Am. Chem. Soc.* **2005**, *127*, 8924–8925.
27. Wang, X. S.; Winnik, M. A.; Manners, I. Swellable, Redox-Active Shell-Crosslinked Organometallic Nanotubes. *Angew. Chem., Int. Ed.* **2004**, *43*, 3703–3707.
28. Wang, X. S.; Wang, H.; Frankowski, D. J.; Lam, P. G.; Welch, P. M.; Winnik, M. A.; Hartmann, J.; Manners, I.; Spontak, R. J. Growth and Crystallization of Metal-Containing Block Copolymer Nanotubes in a Selective Solvent. *Adv. Mater.* **2007**, *19*, 2279–2285.
29. Loverde, S. M.; Klein, M. L.; Discher, D. E. Nanoparticle Shape Improves Delivery: Rational Coarse Grain Molecular Dynamics (rCG-MD) of Taxol in Worm-like PEG-PCL Micelles. *Adv. Mater.* **2012**, *24*, 3823–3830.
30. Geng, Y.; Dalhaimer, P.; Cai, S. S.; Tsai, R.; Tewari, M.; Minko, T.; Discher, D. E. Shape Effects of Filaments *versus* Spherical Particles in Flow and Drug Delivery. *Nat. Nanotechnol.* **2007**, *2*, 249–255.
31. Champion, J. A.; Mitragotri, S. Role of Target Geometry in Phagocytosis. *Proc. Natl. Acad. Sci. U.S.A.* **2006**, *103*, 4930–4934.
32. Fox, M. E.; Szoka, F. C.; Frechet, J. M. J. Soluble Polymer Carriers for the Treatment of Cancer: The Importance of Molecular Architecture. *Acc. Chem. Res.* **2009**, *42*, 1141–1151.
33. Shchepelina, O.; Lisunova, M. O.; Drachuk, I.; Tsukruk, V. V. Morphology and Properties of Microcapsules with Different Core Releases. *Chem. Mater.* **2012**, *24*, 1245–1254.
34. Ye, C. H.; Drachuk, I.; Calabrese, R.; Dai, H. Q.; Kaplan, D. L.; Tsukruk, V. V. Permeability and Micromechanical Properties of Silk Ionomer Microcapsules. *Langmuir* **2012**, *28*, 12235–12244.
35. Shchepelina, O.; Kozlovskaya, V.; Kharlampieva, E.; Mao, W. B.; Alexeev, A.; Tsukruk, V. V. Anisotropic Micro- and Nano-Capsules. *Macromol. Rapid Commun.* **2010**, *31*, 2041–2046.
36. Yan, X. H.; Su, Y.; Li, J. B.; Fruh, J.; Mohwald, H. Uniaxially Oriented Peptide Crystals for Active Optical Waveguiding. *Angew. Chem., Int. Ed.* **2011**, *50*, 11186–11191.
37. Yan, X. H.; Zhu, P. L.; Li, J. B. Self-Assembly and Application of Diphenylalanine-Based Nanostructures. *Chem. Soc. Rev.* **2010**, *39*, 1877–1890.
38. Yah, W. O.; Takahara, A.; Lvov, Y. M. Selective Modification of Halloysite Lumen with Octadecylphosphonic Acid: New Inorganic Tubular Micelle. *J. Am. Chem. Soc.* **2012**, *134*, 1853–1859.
39. Yah, W. O.; Xu, H.; Soejima, H.; Ma, W.; Lvov, Y.; Takahara, A. Biomimetic Dopamine Derivative for Selective Polymer Modification of Halloysite Nanotube Lumen. *J. Am. Chem. Soc.* **2012**, *134*, 12134–12137.

40. Shchukin, D. G.; Mohwald, H. Surface-Engineered Nanocontainers for Entrapment of Corrosion Inhibitors. *Adv. Funct. Mater.* **2007**, *17*, 1451–1458.
41. Li, G. L.; Tai, C. A.; Neoh, K. G.; Kang, E. T.; Yang, X. L. Hybrid Nanorattles of Metal Core and Stimuli-Responsive Polymer Shell for Confined Catalytic Reactions. *Polym. Chem.* **2011**, *2*, 1368–1374.
42. Zhang, Q.; Zhang, T. R.; Ge, J. P.; Yin, Y. D. Permeable Silica Shell through Surface-Protected Etching. *Nano Lett.* **2008**, *8*, 2867–2871.
43. Motornov, M.; Roiter, Y.; Tokarev, I.; Minko, S. Stimuli-Responsive Nanoparticles, Nanogels and Capsules for Integrated Multifunctional Intelligent Systems. *Prog. Polym. Sci.* **2010**, *35*, 174–211.
44. Liu, J. Y.; Pang, Y.; Huang, W.; Zhu, Z. Y.; Zhu, X. Y.; Zhou, Y. F.; Yan, D. Y. Redox-Responsive Polyphosphate Nanosized Assemblies: A Smart Drug Delivery Platform for Cancer Therapy. *Biomacromolecules* **2011**, *12*, 2407–2415.
45. Sevier, C. S.; Kaiser, C. A. Formation and Transfer of Disulphide Bonds in Living Cells. *Nat. Rev. Mol. Cell. Biol.* **2002**, *3*, 836–847.
46. Gao, C. B.; Lu, Z. D.; Yin, Y. D. Gram-Scale Synthesis of Silica Nanotubes with Controlled Aspect Ratios by Templating of Nickel-Hydrazine Complex Nanorods. *Langmuir* **2011**, *27*, 12201–12208.